Proceedings of the ASME 2018
Dynamic Systems and Control Conference
DSCC2018
September 30-October 3, 2018, Atlanta, Georgia, USA

DSCC2018-9187

On the Vibration Suppression and Energy Harvesting of Building Structures Using an Electromagnetic-Inerter-Absorber

Eshagh F. Joubaneh[1], Oumar R. Barry[1, 2], and Lei Zuo[2]
[1]Department of Mechanical Engineering, Central Michigan University, Mount Pleasant, MI 48858, USA
[2]Department of Mechanical Engineering, Virginia Tech, Blacksburg, VA 24060, USA

Abstract

This paper studies the performance of an electromagnetic resonant shunt tuned mass-damper-inerter (ERS-TMDI) in terms of simultaneously suppressing unwanted vibration and harvesting energy in a vibrating building. The ERS-TMDI is attached to a building, which is subjected to an earthquake excitation. An inerter is connected between the TMD and the ground. The electromagnetic transducer and associated circuit, which replaces the viscous damping in the classical tuned mas-damper (TMD), is assumed to be an ideal transducer shunted with a resistor, an inductor, and a capacitor (RLC) circuit. Two RLC circuit configurations are investigated: one in series and another in parallel. The governing equations of motion are presented and H_2 optimization technique is employed to derive explicit expressions for the optimal mechanical tuning ratio, electrical damping ratio, electrical tuning ratio, and electromagnetic mechanical coupling coefficient. The validity of the obtained closed-form expressions is examined using Matlab optimization toolbox. Parametric studies are carried out to investigate the effect of the mass and inertance ratios on the obtained optimal parameters. Numerical examples are also conducted to demonstrate the role of key design variables on vibration mitigation and energy harvesting performances. Also, the performance of a parallel RLC circuit configuration is compared to that of a series configuration.

INTRODUCTION

Many engineering structures such as bridges, airplanes, powerlines, and cars usually suffer from unwanted vibrations, which can result in fatigue failure or human discomfort. Tuned Mass Damper (TMD) is one of the most common passive control devices for suppressing the unwanted vibrations [1-3]. It consists of a mass with a spring and a viscous damper that is attached to the main structure. The vibration suppression mechanism is achieved by transferring the kinetic energy of the main structures to the tuned mass through a spring and damper. This energy is then dissipated through the TMD device as heat [4–7].

Many studies have been conducted to optimize the design of TMDs using different criterion; such as, the fixed point, H_2 and H_∞. Den Hartog [8] and Brock [9] are among the first scholars who presented explicit mathematical expressions for optimizing stiffness and damper using the "fixed point" theory. Asami et. al also presented analytical solution for the optimization of a dynamic vibration absorbers (DVA) using H_2 and H_∞ optimization criteria [10-11]. Tuned mass damper (TMD) has also been applied to continuous systems to dissipate the vibration amplitude of plates and beams [12].

Numerous investigators have incorporated electromagnetic and/or piezoelectric transducers in TMDs for simultaneously harvesting energy and suppressing vibration [13]. A general technique for larger scale energy harvesting and vibration control is to replace or to complement the mechanical damping element by an electromagnetic device so that all the energy is not dissipated through the device as wasted heat, but rather the energy is recovered electrically and then stored in batteries. The generated energy can then be used to achieve self-powered semi-active/active vibration control or/and to power wireless sensors for structural health monitoring [14-17].

To this end, this paper presents analytical and numerical investigations of the optimal design parameters of an electromagnetic resonant shunt tuned mass-damper-inerter (ERS-TMDI) attached to a building, which subjected to a ground excitation. The H_2 norm criterion is used to obtain closed-form analytical expressions for the optimal design parameters of the system in order to simultaneously mitigate the vibrations of the

primary structure and harvest energy. The obtained mathematical expressions for the optimal mechanical tuning ratio, electrical damping ratio, electrical tuning ratio, and electromagnetic mechanical coupling coefficient are compared with those obtained using Matlab optimization tool box. Parametric studies are conducted to examine the role of key design parameters on the vibration mitigation of the primary structure and harvested electrical power. Also, the performance of parallel RLC circuit is compared with that of the series configuration.

Mathematical Modeling

Figure 1 depicts a schematic of a single degree freedom system consisting of primary structure m_s with a linear spring stiffness k_s, and damping coefficient c_s. The primary structure is coupled with the ERS-TMDI of mass m_T and stiffness k_T. The inertance of the system, denoted by b, is grounded at one end and connected to the absorber mass at the other end. An ideal electromagnetic transducer is connected in parallel with the stiffness k_T, between the primary structure and the mass m_T. The transducer will be shunt with RLC circuits in parallel or in series. We assume the back electromotive voltage and force constants are k_V and k_f. The resistance, capacitance, and inductance of the electrical circuit are denoted by R, C, and L, respectively. The electric circuit in series configuration is depicted in Figure1 (a) and the parallel configuration is shown in Figure 1 (b).

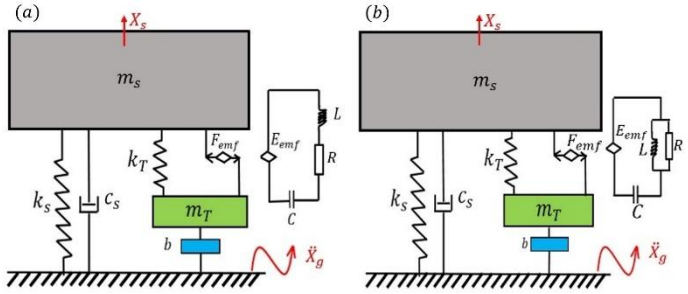

Figure1. Schematic of Host structure with ERS-TMDI absorber; (a) series circuit, (b) parallel circuit.

The governing equation of motion of the coupled system with series circuit subjected to ground acceleration $\ddot{x}_g$ caused by earthquake can be obtained as

$$m_s\ddot{x}_s + c_s\dot{x} + k_s x_s - k_T(x_T - x_s) + k_f I = -m_s\ddot{x}_g$$

$$(m_T + b)\ddot{x}_T + k_T(x_T - x_s) - k_f I = -(m_T + b)\ddot{x}_g$$

$$k_v(\dot{x}_T - \dot{x}_s) + RI + L\dot{I} + \frac{1}{C}\int I dt = 0 \qquad (1)$$

Applying Laplace transform into Eq. (1) and considering the primary structure undamped, the equations of motion become

$$(m_s s^2 + k_s + k_T)X_s - k_T X_T + k_f I = -m_s\ddot{X}_g$$

$$-k_T X_s + \big((m_T + b)s^2 + k_T\big)X_T - k_f I = -(m_T + b)\ddot{X}_g$$

$$-k_v s X_s + k_v s X_T + RI + LIs + \frac{I}{CS} = 0 \qquad (2)$$

Considering the normalized frequency $s = j\omega$, the third equation of Eq. (2) can be written as

$$I = \frac{K_S}{K_f} q_1 (X_S - X_T) \qquad (3)$$

where q_1

$$q_1 = \frac{f_T^2 \mu \mu_k (j\alpha)^2}{(j\alpha)^2 + 2\zeta_e f_e (j\alpha) + f_e^2} \qquad (4)$$

For the parallel RLC configuration Eq. (3) changes to

$$I = \frac{K_S}{K_f} \frac{\mu_k f_T^2 \mu [(j\alpha)^3 + 2\zeta_e f_e (j\alpha)^2]}{2\zeta_e f_e (j\alpha)^2 + f_e^2 (j\alpha) + 2\zeta_e f_e^3} (X_S - X_T) \qquad (5)$$

Substituting Eq. (3) into Eq. (2) we obtain

$$[(j\alpha)^2 + (1 + f_T^2\mu) + q_1]X_s - (f_T^2\mu + q_1)X_T = -\frac{\ddot{X}_g}{\omega_s^2}$$

$$[-f_T^2\mu - q_1]X_s + [(1 + \delta)\mu(j\alpha)^2 + f_T\mu + q_1]X_T = -\psi\mu\frac{\ddot{X}_g}{\omega_s^2} \qquad (6)$$

The parameters used in the dynamic of the system are defined in Table 1.

Table 1. Definitions of parameter s used in the dynamic equations

Data	Definition
$\boldsymbol{\omega_s = \sqrt{k_s/m_s}}$	Natural frequency of the primary structure
$\boldsymbol{\omega_T = \sqrt{k_T/m_T}}$	Natural frequency of the tuned mass
$\boldsymbol{\omega_e = 1/\sqrt{LC}}$	Resonant natural frequency of the circuit
$\boldsymbol{\mu = m_T/m_s}$	Mass ratio of the tuned mass to the primary structure
$\boldsymbol{\delta = b/m_T}$	Mass ratio of the inertance to the primary structure
$\boldsymbol{f_T = \omega_T/\omega_s}$	Mechanical tuning ratio
$\boldsymbol{f_e = \omega_e/\omega_s}$	Electrical tuning ratio
$\boldsymbol{\alpha = \omega/\omega_s}$	Normalized frequency
R	Resistance
$\boldsymbol{\zeta_e = R/(2L\omega_e)}$	Electrical damping ratio
$\boldsymbol{\mu_k = k_f k_v/k_T L}$	Electromagnetic mechanical coupling coefficient
$\boldsymbol{k_v}$	Voltage constant of the transducer
$\boldsymbol{k_f}$	Force constant of the transducer

H_2 Optimization for the ERS-TMDI

Following [18], the optimum parameters of f_T, f_e, μ_k and ζ_e to minimize the vibrations of the primary structure (x_s) caused by the ground excitation, $\ddot{x}_g/\omega_s^2$ can be obtained as follows

$$PI = \frac{1}{2\pi}\int_{-\infty}^{\infty} \left|\frac{X_s(j\alpha)}{\ddot{X}_g(j\alpha)/\omega_s^2}\right|^2 d\alpha \qquad (7)$$

Where $X_s(j\alpha)/\ddot{X}_g(j\alpha)/\omega_s^2$ is the normalized transfer function and is given as

$$\frac{X_s(j\alpha)}{\ddot{X}_g(j\alpha)/\omega_s^2} = \frac{B_4(j\alpha)^4+B_3(j\alpha)^3+B_2(j\alpha)^2+B_1(j\alpha)+B_0}{A_6(j\alpha)^6+A_5(j\alpha)^5+A_4(j\alpha)^4+A_3(j\alpha)^3+A_2(j\alpha)^2+A_1(j\alpha)+A_0} \tag{8}$$

Where

$$\begin{cases} A_6 = \psi \\ A_5 = 2\psi f_e\zeta_e \\ A_4 = f_t^2(\mu_k + 1)(\mu\psi + 1) + \psi + f_e^2\psi \\ A_3 = 2f_e\psi\zeta_e + 2f_e f_t^2\zeta_e(1+\mu\psi) \\ A_2 = f_e^2\psi + f_t^2(1+\mu_k) + f_e^2 f_t^2(1+\mu\psi) \\ A_1 = 2f_e f_t^2\zeta_e \\ A_0 = f_e^2 f_t^2 \end{cases}$$

$$\begin{cases} B_4 = \psi \\ B_3 = 2\psi f_e\zeta_e \\ B_2 = f_t^2(\mu_k + 1)(\mu\psi + 1) + f_e^2\psi \\ B_1 = 2(1+\mu\psi)f_e f_t^2\zeta_e(j\alpha) \\ B_0 = f_e^2 f_t^2(1+\mu\psi) \end{cases} \tag{9}$$

where $\psi = \delta + 1$. Applying the residue theorem [19] into Eq. (7), the performance index (PI) can be obtained as

$$PI = \frac{1}{4f_e f_t^2\mu\mu_k\psi^2\zeta_e}\{f_e^4[f_t^4(\mu^5\psi^5 + 5\mu^4\psi^4 + 10\mu^3\psi^3 + 10\mu^2\psi^2 + 5\mu\psi + 1) + f_t^2(2\mu^4\psi^5 + 4\mu^3\psi^4 - 4\mu\psi^2 - 2\psi) + \mu^3\psi^5 + \psi^2] + f_e^2(-2f_t^4\mu^4\mu_k\psi^4 + 4f_t^4\mu^4\psi^4\zeta_e^2 - 2f_t^4\mu^4\psi^4 - 8f_t^4\mu^3\mu_k\psi^3 + 16f_t^4\mu^3\psi^3\zeta_e^2 - 8f_t^4\mu^3\psi^3 - 12f_t^4\mu^2\mu_k\psi^2 + 24f_t^4\mu^2\psi^2\zeta_e^2 - 12f_t^4\mu^2\psi^2 - 8f_t^4\mu\mu_k\psi + 16f_t^4\mu\psi\zeta_e^2 - 8f_t^4\mu\psi - 2f_t^4\mu_k + 4f_t^4\zeta_e^2 - 2f_t^4 - f_t^2\mu^3\mu_k\psi^4 + 4f_t^2\mu^3\psi^4\zeta_e^2 - 2f_t^2\mu^3\psi^4 + 3f_t^2\mu\mu_k\psi^2 - 12f_t^2\mu\psi^2\zeta_e^2 + 6f_t^2\mu\psi^2 + 2f_t^2\mu_k\psi - 8f_t^2\psi\zeta_e^2 + 4f_t^2\psi + 4\psi^2\zeta_e^2 - 2\psi^2) + f_t^4(\mu^3\mu_k^2\psi^3 + 2\mu^3\mu_k\psi^3 + \mu^3\psi^3 + 3\mu^2\mu_k^2\psi^2 + 6\mu^2\mu_k\psi^2 + 3\mu^2\psi^2 + 3\mu\mu_k^2\psi + 6\mu\mu_k\psi + 3\mu\psi + \mu_k^2 + 2\mu_k + 1) + f_t^2(-2\mu\mu_k\psi^2 - 2\mu\psi^2 - 2\mu_k\psi - 2\psi) + \psi^2\} \tag{10}$$

Setting the derivation of PI with respect to design parameters equal to zero we obtain

$$\frac{\partial PI}{\partial f_t} = 0 \quad \frac{\partial PI}{\partial f_e} = 0 \quad \frac{\partial PI}{\partial \mu_k} = 0 \quad \frac{\partial PI}{\partial \zeta_e} = 0 \tag{11}$$

By solving these four equations, the optimal parameters for series case can be obtained as

$$f_t = \frac{\sqrt{\psi(4-3\mu\psi)}}{2(\mu\psi+1)} \quad f_e = \sqrt{\frac{16-9\mu\psi}{3\mu^2\psi^2+19\mu\psi+16}}$$

$$\mu_k = \frac{128\mu\psi}{64-36\mu\psi-9\mu^2\psi^2} \qquad \zeta_e = \sqrt{\frac{192\mu\psi}{256-96\mu\psi-27\mu^2\psi^2}} \tag{12}$$

The instant power due to the external load can be found as

$$P = R_e I^2 \tag{13}$$

The normalized transfer function from $\ddot{X}_g/\omega_s^2$ to I is given as

$$I_n = \frac{I(j\alpha)}{\ddot{X}_g(j\alpha)/\omega_s^2} = \frac{\frac{K_v}{L}\psi(j\alpha)^2}{A_6(j\alpha)^6+A_5(j\alpha)^5+A_4(j\alpha)^4+A_3(j\alpha)^3+A_2(j\alpha)^2+A_1(j\alpha)+A_0} \tag{14}$$

Using Eqs. (13) and (14), the normalized frequency function from $\ddot{X}_g/\omega_s^2$ to $\sqrt{P}$ can be written as

$$P_n = \frac{I_n\sqrt{R_e}}{\ddot{X}_g(j\alpha)/\omega_s^2} \tag{15}$$

Numerical Analysis

The validation of the obtained optimal expressions is demonstrated in Table 3. This is realized by comparing the results obtained using Equation (12) to those obtained numerically using Matlab optimization toolbox for a fixed mass ratio $\mu = 0.02$ and various inertance ratios. The results are presented in Table 3 and show very good agreement. To further illustrate the validity of the proposed closed form expressions, Figure 2 shows the optimal frequency response curves obtained analytically using Equation (12) and numerically using Matlab optimization toolbox. The results collaborate perfectly. This is an indication that the derived closed-form expressions for the optimal parameters are valid and can be used to facilitate the optimal design of ERS-TMDI. It can also be observed that ERS-TMDI has better performance in comparison with the classic TMD for the same mass ratio ($\mu = 0.02$).

Table 3: Designed parameters presented for the ERS-TMDI system with mass ratio $\mu = 0.02$ by analytical and numerical methods.

Type	Data	f_t	f_e	μ_k	ζ_e
$\delta = 0.1$	**Analytical**	1.018	0.981	0.044	0.129
	Matlab	1.018	0.981	0.044	0.129
$\delta = 0.5$	**Analytical**	1.176	0.974	0.060	0.151
	Matlab	1.176	0.974	0.060	0.151
$\delta = 1$	**Analytical**	1.339	0.966	0.080	0.174
	Matlab	1.339	0.966	0.080	0.174

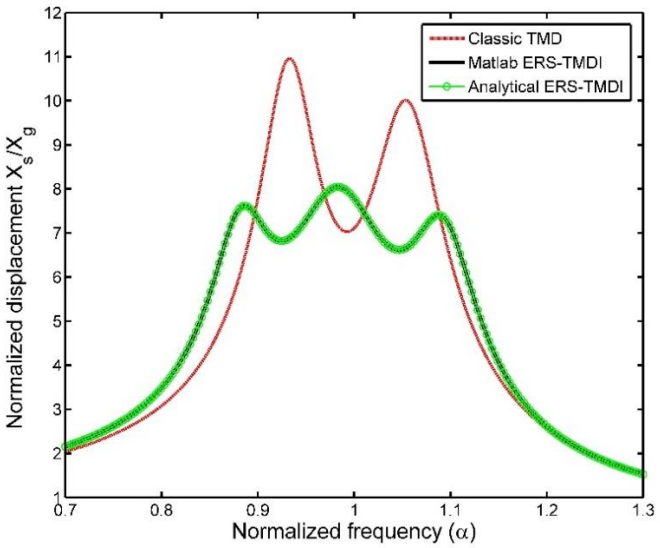

Figure 2: Optimal frequency response under mass ratio $\mu = 0.02$ and inertance ratio: $\delta = 0.1$ by analytical and numerical simulation for ERS-TMDI and comparison with classic TMD under mass ratio $\mu = 0.02$ and $b = 0$.

Figure 3 depicts three-dimensional representation of performance index (PI) with respect to electromagnetic mechanical coupling coefficient μ_k and electrical damping ratio. It can be observed that electromagnetic mechanical coupling coefficient μ_k is more effective on changing the performance index.

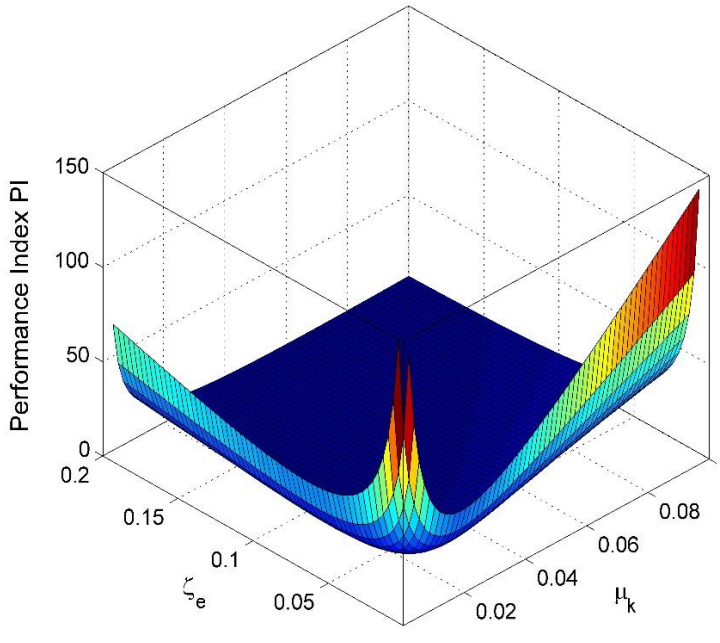

Figure 3. Three-dimensional representation of performance index (PI) with respect to electromagnetic mechanical coupling coefficient μ_k and electrical damping ratio ζ_e under $\mu = 0.02, \delta = 0.1, f_t = 1.018$, and $f_e = 0.981$.

Figure 4 depicts the variation of optimum parameters with respect to mass and inertance ratios in a three-dimensional representation. It can be observed that the electromagnetic mechanical coupling coefficient and electrical damping ratio increase with increasing both mass and inertance ratios. The electrical tuning ratio decreases with increasing both mass and inertance ratios. The mechanical tuning ratio decreases with increasing mass ratio, but it increases with increasing inertance ratio.

(a)

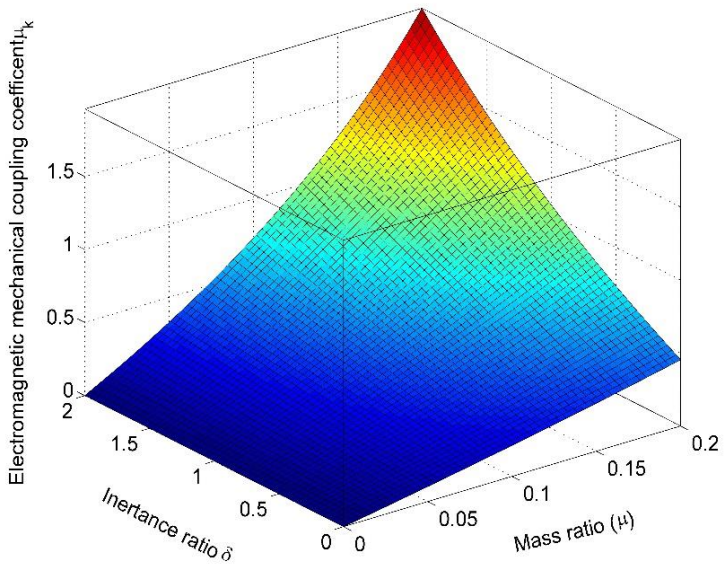

(b)

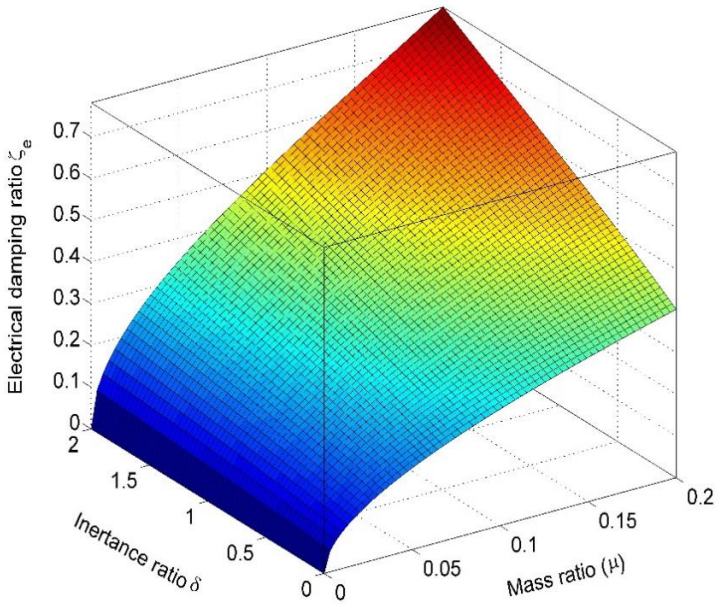

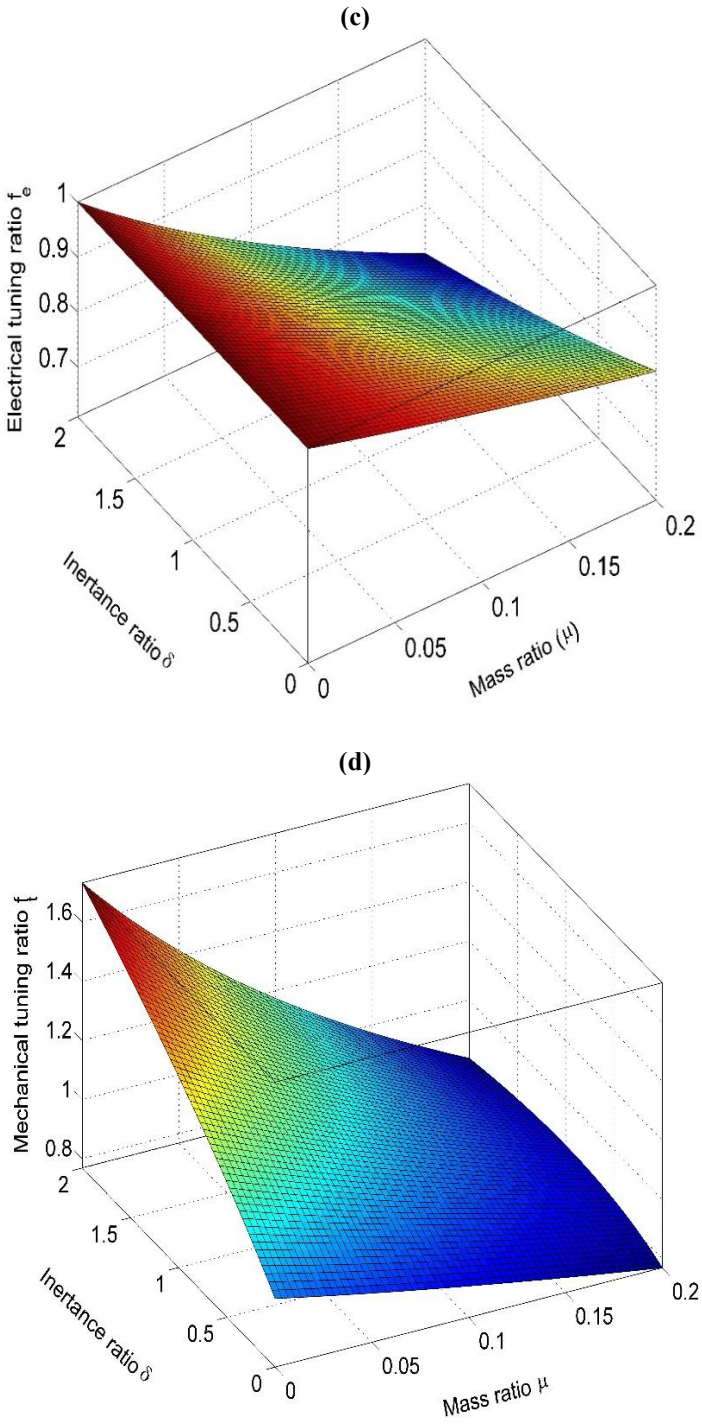

Figure 4. Variation of optimal parameters; (a) electromagnetic mechanical coupling coefficient μ_k, (b) electrical damping ratio ζ_e, (c) electrical tuning ratio f_e (d) mechanical tuning ratiof_T with respect to inertance ratio δ and mass ratio μ.

To better understand the role of the optimal parameters with respect to mass and inertance ratios, two-dimensional graphs are presented in Figure 5. The results indicate that as the mass ratio increases, the effects of the inertance ratio is more significant on the electromagnetic mechanical coupling coefficient, electrical damping ratio, and electrical tuning ratio; whereas the effect of the inertance ratio on the mechanical tuning ratio becomes less pronounced.

Figure 6 depicts the normalized displacement of the primary structure X_s/X_g and relative displacement $(X_S - X_T)/X_g$. It can be observed that both normalized displacements decrease with increasing inertance ratio δ. This figure also shows that ERS-TMDI system exhibits better performance in terms of vibration mitigation of the primary structure as compared to the EMTMD system studied in [18]. Figure 7 shows that the harvested power increases with increasing inertance ratio. Also, the results in this figure clearly show that the harvested power from the ERS-TMDI is significantly higher than that of EMTMD ($\delta = 0$)system studied in [18].

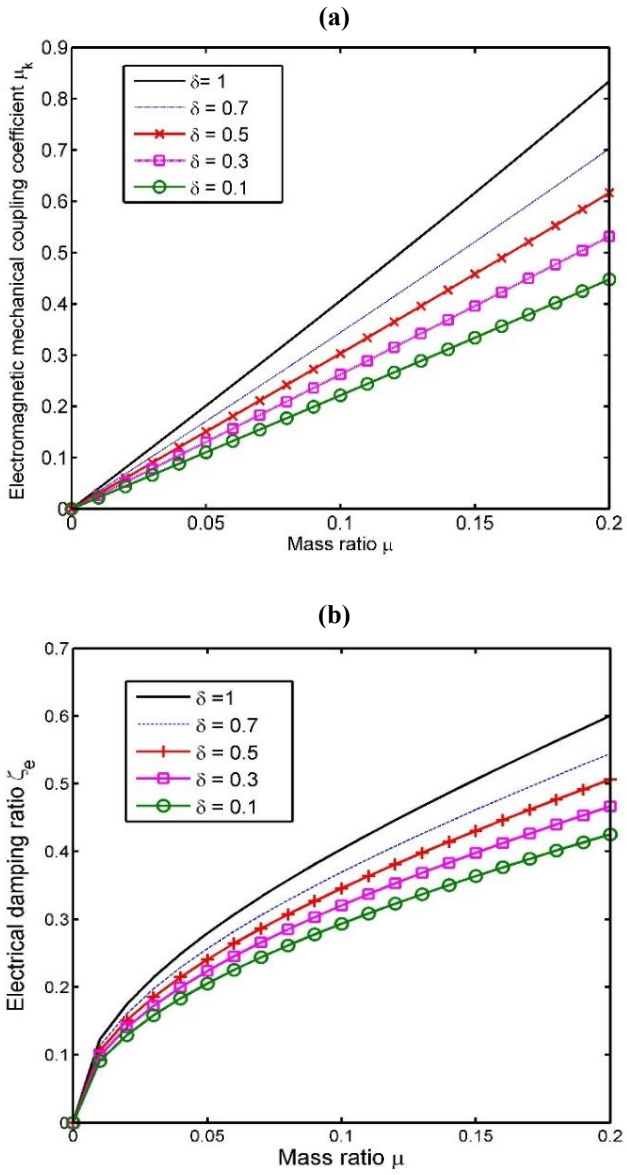

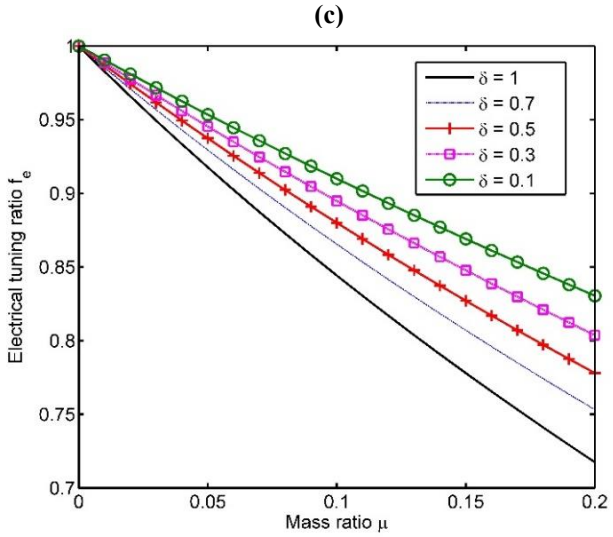

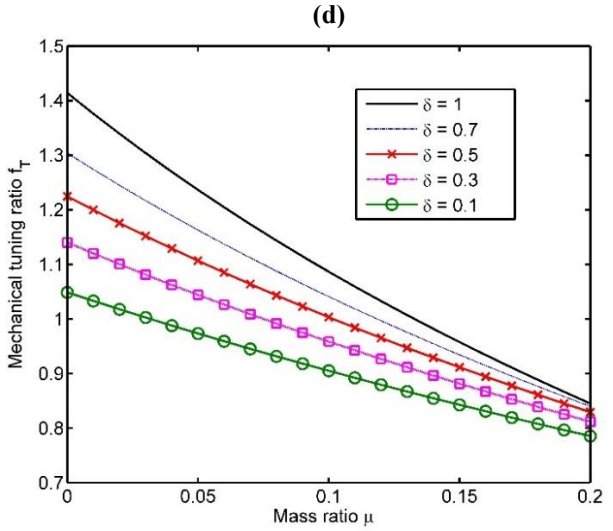

Figure 5. Two-dimensional graphical representations of optimum parameters; (a) optimal electromagnetic mechanical coupling coefficient μ_k, (b) optimal electrical damping ratio ζ_e, (c) optimal electrical tuning ratio f_e (d) Optimal mechanical tuning ratio f_T.

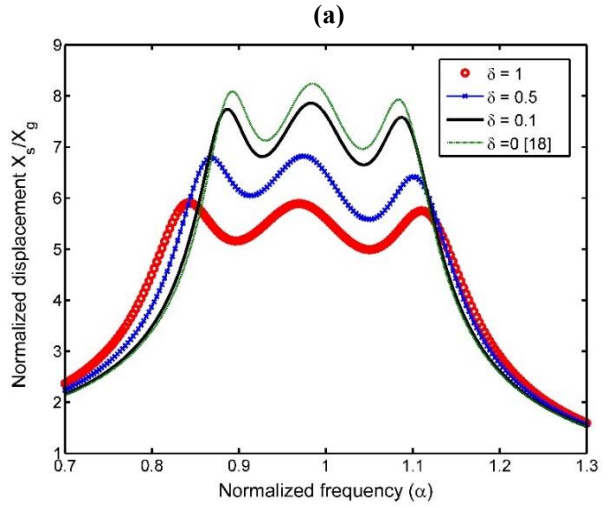

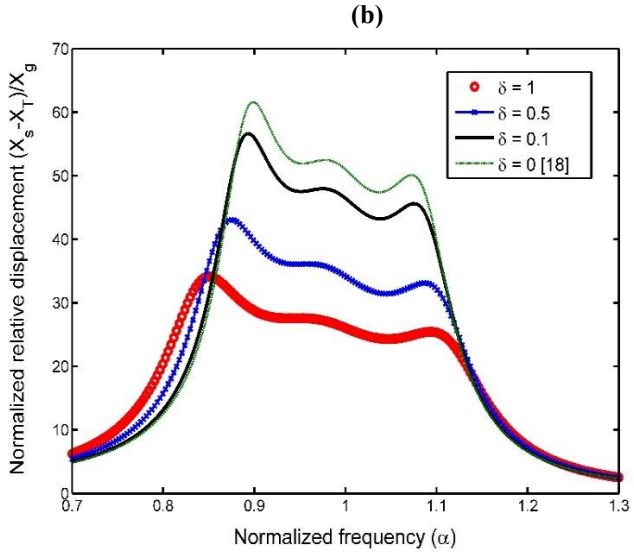

Figure 6. Schematic of the optimal frequency response under mass ratio $\mu = 0.02$ and different inertance ratio: (a) the deformation of the primary structure and (b) the relative deformation of the ERS-TMDI.

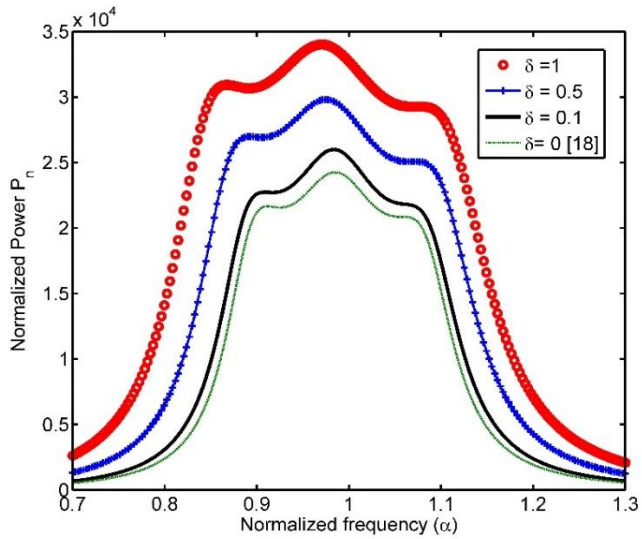

Figure 7. Comparison of normalized power for different inertance ratio and with the mass ratio $\mu = 0.02$. $k_v = 150, L = 1.17H, R_e = 0.1\ \Omega$.

Figures 8 and 9 compare the performance of parallel and series RLC circuit configurations in terms of vibration mitigation and energy harvesting, respectively. As it can be observed from Figure 8, the two configurations exhibit almost the same vibration amplitude throughout the whole frequency range. This is an indication that these two configurations have similar performance in terms of vibration mitigation. However, in terms of energy harvesting performance as shown in Figure 9, the parallel RLC configuration performs much better than the series RLC configuration.

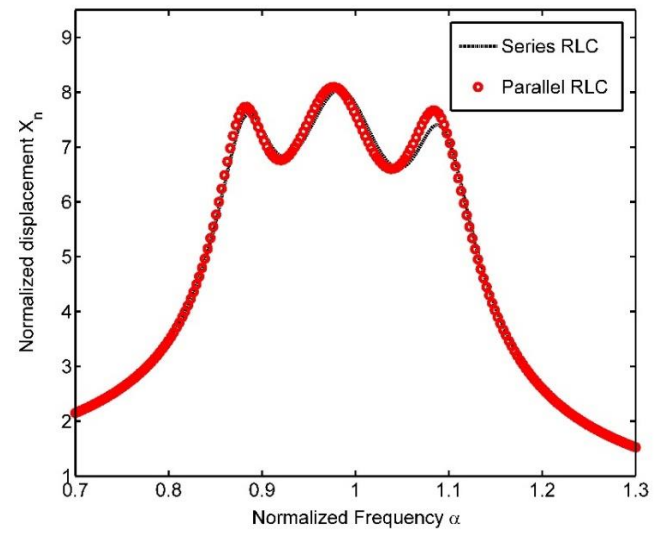

Figure 8: Comparison of normalized deformation of primary structure with series and parallel RLC configurations, $\mu = 0.02$ and inertance ratio: $\delta = 0.1$.

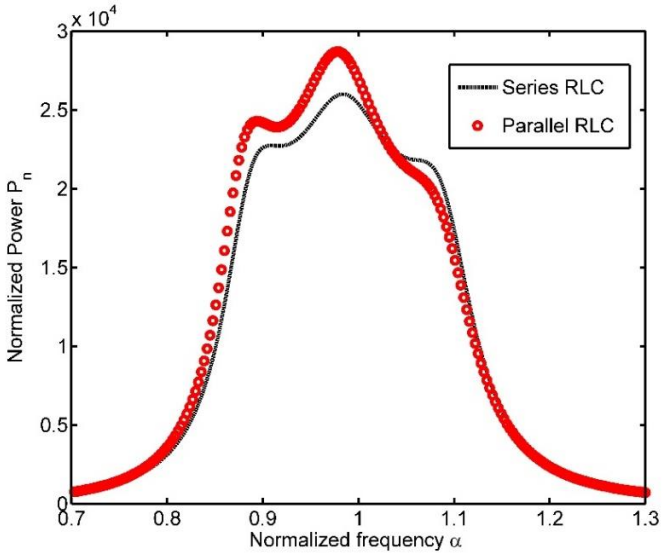

Figure 9: Comparison of normalized power of ERS-TMD for different RLC circuits using $\mu = 0.02$ and inertance ratio $\delta = 0.1$.

Conclusion

In this paper, we presented closed form expressions for the optimal design parameters of an ERS-TMDI system using H_2 norm criteria. The ERS-TMDI is attached to a building, which is subjected to an earthquake excitation. The goal of the ERS-TMDI is to simultaneously suppress unwanted vibration and harvest energy of the vibrating building. The accuracy of the obtained optimal expressions is examined numerically using Matlab optimization toolbox. The results show very good agreement. These optimal parameters, namely: electromagnetic mechanical coupling coefficient μ_k, electrical damping ratio ζ_e, electrical tuning ratio f_e, and mechanical tuning ratio f_t are all dependent on the mass and inertance ratios.

Parametric studies are carried out to examine the effect of mass and inertance ratios on the obtained optimal design parameters. The results show that increasing the mass and inertance ratios both increase the electromagnetic mechanical coupling coefficient and electrical damping ratio. The effect of the inertance ratio on both aforementioned optimal parameters is more pronounced as the mass ratio increases. Increasing the mass and inertance ratios both decrease the electrical tuning ratio and this decreasing effect is more significant for larger mass ratio. Increasing the mass ratio decreases the mechanical tuning ratio; whereas, increasing the inertance ratio increases the mechanical tuning ratio. The effect of the inertance ratio on the mechanical tuning parameter is more significant for smaller mass ratios. The role of the inertance ratio on the vibration mitigation and harvesting energy performances indicate that increasing the inertance ratio increases the performance of ERS-TMDI in terms of both vibration mitigation and energy harvesting. Numerical examples also demonstrate that parallel RLC configuration exhibits superior performance than series RLC configuration in terms of energy harvesting and similar performance in terms of vibration mitigation. The authors anticipate future work to be focused on various ERS-TMDI topologies with experimental validations.

References

[1] Frahm, H., Device for Damping Vibrations of Bodies, U.S. Patent, No. 989, 958, 3576–3580, 1911.

[2] Den Hartog JP., Mechanical Vibrations, McGraw-Hill, 4th ed., 1956.

[3] Salvi J, Rizzi E., Closed-form optimum tuning formulas for passive Tuned Mass Dampers under benchmark excitations, Smart Structures and Systems, 17(2): 231–256, 2016.

[4] Krenk S., Frequency Analysis of the Tuned Mass Damper, Journal of Applied Mechanics (ASME), 72(6):936– 942, 2005.

[5] Bakre S.V., Jangid R.S., Optimum parameters of tuned mass damper for damped main system, Structural Control and Health Monitoring, 14(3):448–470, 2006.

[6] Salvi J., Rizzi E., Optimum tuning of Tuned Mass Dampers for frame structures under earthquake excitation, Structural Control and Health Monitoring, 22(4):707–725, 2015.

[7] Salvi J., Rizzi E., Rustighi E., Ferguson NS. On the optimisation of a hybrid Tuned Mass Damper for impulse loading, 2015.

[8] Ormondroyd, J. and Den Hartog, J.P., Theory of the dynamic vibration absorber, Transactions of the American Society of Mechanical Engineers, vol. 50, 9–22, 1928.

[9] Brock J. E., A note on the damped vibration absorber, Journal of Applied Mechanics, vol. 68, A-284, 1946.

[10] Asami T., Nishihara. O, Baz. A.M., Analytical solution to H_∞ and H_2 optimization of dynamic vibration absorbers attached to damped linear systems, vol. 124, 2002.

[11] Asami T., Optimal design of double-mass dynamic vibration absorbers arranged in series or in parallel, Journal of Vibration and Acoustics, vol. 139, 2017.

[12] Cheung Y.L., Wong, W.O. H_∞ and H_2 optimizations of a dynamic vibration absorber for suppressing vibration in plates, Journal of Vibration and Acoustics, vol. 124, 284-295, 2002.

[13] Liu, Y., Design, Modeling and Control of Vibration Systems with Electromagnetic Energy Harvesters and their Application to Vehicle Suspensions (Doctoral dissertation, Virginia Tech), 2016.

[14] Scruggs, J., and Lindner, D. K., Active energy control in civil structures. In 1999 Symposium on Smart Structures and Materials, International Society for Optics and Photonics, 194-205, 1999.

[15] Scruggs J. T., and Iwan W. D., Control of a civil structure using an electric machine with semiactive capability. Journal of Structural Engineering, 129(7), 951-959, 2003.

[16] Luo Y., Sun H., Wang X., Zho L., Chen N., Wind Induced Vibration Control and Energy Harvesting of Electromagnetic Resonant Shunt Tuned Mass-Damper-Inerter for Building Structures, 4180134-1-13, 2017.

[17] Gonzalez-Buelga A., Clare L. R., Cammarano A., Neild S. A., Burrow S. G., and Inman D. J., An optimized tuned mass damper/harvester device, Structural Control and Health Monitoring, 21(8), 1154–1169, 2014.

[18] Liu. Y., Lin C.-C., Parker J., Zuo L., Exact H_2 optimal tuning and experimental verification of energy-harvesting series electromagnetic tuned-mass dampers, Journal of Vibration and Acoustics, vol. 138, (061003-1-12), 2016.

[19] Gradshteyn I. and Ryzhik I., Table of Integrals Series and Product, Academic Press, 1980.